

Self-assembly of Phenylalanine-Leucine Leucine-Phenylalanine and Cyclo(-Leucine- Phenylalanine) Dipeptides through Simulations and Experiments

Peter Divanach^{1,2}, Eirini Fanouraki¹, Anna Mitraki^{1,2*},

Vagelis Harmandaris^{3,4,5}, Anastassia N. Rissanou^{5,6,*}

1. Department of Materials Science and Technology, University of Crete, GR-70013, Voutes Campus Greece.
2. Institute of Electronic Structure and Laser / Foundation for Research and Technology-Hellas, (FORTH), Nikolaou Plastira 100, GR-71110, Vassilika Vouton, Heraklion, Crete, Greece
3. Institute of Applied and Computational Mathematics (IACM), Foundation for Research and Technology Hellas, (FORTH), IACM/FORTH, GR-71110 Heraklion, Crete, Greece.
4. Department of Mathematics and Applied Mathematics, University of Crete, GR-71409, Heraklion, Crete, Greece.
5. Computation-based Science and Technology Research Center; The Cyprus Institute, Nicosia 2121, Cyprus.
6. Natl Hellen Res Fdn, Theoret & Phys Chem Inst, 48 Vassileos Constantinou Ave, Athens 11635, Greece.

Keywords: Dipeptides; self-assembly; architecture; molecular dynamics; field emission scanning electron microscopy; Phenylalanine; Leucine

Correspondence to: trissanou@eie.gr (A.N.R.), mitraki@materials.uoc.gr (A.M.)

Abstract

For over two decades, peptide self-assembly has been the focus of attention and a great source of inspiration for biomedical and nano-technological applications. The resulting peptide nanostructures and their properties, are closely related to the information encoded within each peptide building block, their sequence and their modes of self-organization. In this work we assess the behavior and differences between the self-association of the aromatic-aliphatic Phe-Leu dipeptide compared to its retro-sequence Leu-Phe and cyclic Cyclo(-Leu-Phe) counterparts using a combination of simulation and experimental methods. Detailed all-atom molecular dynamics (MD) simulations offer a quantitative prediction at the molecular level of the conformational, dynamical and structural properties of the peptides' self-assembly, while field emission scanning electron microscopy (FESEM) experiments allow microscopic observation of the self-assembled end-structures. The complementarity and qualitative agreement between the two methods not only highlights the differences between the self-assembly propensity of cyclic and linear retro-sequence peptides but also sheds light on underlying mechanisms of self-organization. The self-assembling propensity was found to follow the order: Cyclo(-Leu-Phe) > Leu-Phe > Phe-Leu.

I. Introduction

Self-assembly is a process encountered in all living systems, which creates degrees of order in otherwise disordered systems and allows them to function. Self-assembling peptides tend to undergo spontaneous assembly into ordered, biocompatible nanostructures, under mild conditions, through weak, yet powerful non-covalent interactions. For the last decades, peptide self-assembly has been the subject of much attention and inspiration partially due the enormous potential for scientific and technological applications but also due to the basic scientific questions surrounding it in relation to the origin of life itself.¹ The most well-studied dipeptide, the diphenylalanine (Phe-Phe) one, first introduced by Gazit, Reches et al., is known to self-assemble into ordered nanotubes in the presence of water² with unique mechanical, optical and electrical properties³. Not only is diphenylalanine an excellent model candidate for understanding key-elements of the self-assembly process given the extensive theoretical and experimental studies conducted on it^{4, 5}, but it also constitutes an ideal reductionist model for studying amyloid formation as the minimal recognition motif of the amyloid-beta peptide sequence KLVFFAE (residues 17–23)⁶.

While aromatic phenylalanine rings are believed to be of vital importance to the assembly process through π - π^* stacking interactions^{7, 8}, they constitute one piece of a larger puzzle, as peptides rich in aliphatic amino acids also self-assemble efficiently into amyloid-type fibrils, with the GAIG sequence being a primary example^{9, 10}. Aliphatic peptide crystals can also function as novel materials, exhibiting high permeability and selectivity, with gas storage applications and sorption-release potential¹¹⁻¹⁶

The above interesting properties however, are not exclusive to peptides composed of solely aromatic or aliphatic amino acids, but extend to peptides containing combinations of aromatic with aliphatic amino acids. The distinct property of the mixed aromatic-aliphatic peptides is their frequent presence in neuropeptide sequences¹⁷. The Phe-Leu motif is the C-terminal motif in the Leu-enkephalin (Tyr-Gly-Gly-Phe-Leu) and is also present in the sequences of dynorphin, and α and β neoendorphins¹⁸. Moreover, Phe-Leu based dipeptide and tripeptide drugs act as proteasome inhibitors and are used for the treatment of multiple myeloma. Furthermore, dipeptide structures comprised of an aromatic amino acid combined with Leucine seem to display antidepressant¹⁹ and anxiolytic activity in mice while interestingly, their retro-sequence counterparts do not seem to exhibit such behavior²⁰. The effect of amino acid

sequence is mainly met in proteins, where the protein folding problem is based on it.²¹ However, this is apparent even in dipeptides where it affects their behavior in aqueous solutions.

As such, the challenging task of unraveling the mechanisms governing self-assembly is best approached by analyzing how various factors affect the end morphologies²². These comprise the effect of the environment (solvent, temperature, etc.)⁴, as well as the physico-chemical nature of the peptides, including their termini and side groups, the presence or absence of protective groups and the types of specific interactions. In general, three main classes of peptide geometries can be distinguished, i.e. linear, stapled, cyclic ones, or variations of the above²³. Cyclic peptides contain a circular sequence of bonds and can be either natural²⁴ or synthetic²⁵, ranging from two to hundreds of amino acids long. These kinds of peptides tend to display improved binding affinity, specificity and stability due to their entropic advantage²⁶ and are less prone to proteolysis compared to their more flexible, linear analogues. The elimination of the charged termini in cyclic peptides often endows them with enhanced membrane permeability and the reduced conformational freedom they exhibit, usually prevents off-target side effects during drug-delivery. Their greatest assets however can also prove to be a double-edged blade, as the flexibility of the linear parent structure may at times be required, especially in the case of certain target-receptors or biodegradable scaffolds²⁷. Moreover a lot of cyclic-peptides constitute excellent gelators²⁸, with a lot of comparisons focusing on various cyclic dipeptides including Cyclo(-Leu-Phe)^{29,30} in different solvents. S. Marchesan et al. have even performed extensive studies on the gelation capacities between stereoisomers, structural isomers and linear and cyclic dipeptides^{31,32}. Furthermore, diketopiperazines and various other cyclic dipeptides act as chiral catalysts or precursors in prebiotic processes³³, they have cancer targeting applications when compared to linear ones³⁴ and they are considered as valuable minimal models for explaining the origins of life. Thus, a lot of comparisons are being performed, both experimental³² theoretical³⁵ and through combined experimental and computational studies³⁶ amongst different kinds of cyclic peptides and the different capacities of their various morphologies with entire libraries being dedicated to them³⁵.

It is therefore imperative to properly assess the self-assembling tendencies of both linear and cyclic peptide analogues in order to select the most suitable for each application. This challenging, yet necessary task of correlating both the nature and outcome of the self-assembly

process with the information encoded within each molecular building block can be optimally tackled using a combination of experimental and theoretical approaches^{4, 37}. As an example, Arnon et al³⁸ used a mixture of Monte Carlo and implicit solvent MD simulations on parts of the crystalline assemblies of diphenylalanine (Phe-Phe) and Cyclo-diphenylalanine [Cyclo(-Phe-Phe)], to interpret their respective unidirectional and bidirectional growth, while also measuring and directing their elongation using micro-fluidics. Other computational comparisons have also been performed by J. Jeon et al³⁹ in order to postulate on the tendency of vapor-deposited in vacuum diphenylalanine to dehydrate, crystallize into Cyclo-diphenylalanine and produce hydrophobic rod-like assemblies, as opposed to the usual hollow nanotubes yielded in water⁴⁰. Direct MD comparisons between linear and cyclic peptides have often been performed, much like the case of Arg-Gly-Asp peptide motif and its interactions with integrin $\alpha_v\beta_3$ ⁴¹, or in the cases of the opioid (D-Pen2,D-Pen5)-Enkephalin (Pen standing for penicillamine)⁴² where the conformational flexibility of both cyclic and non-cyclic analogues was investigated in an effort to link calculated properties to their biological functions.

The present study refers to a thorough investigation of the structural and conformational properties of three specific mixed aromatic-aliphatic dipeptides, namely Phenylalanine-Leucine (Phe-Leu), Leucine-Phenylalanine (Leu-Phe) and Cyclo(-Leucine-Phenylalanine-) [Cyclo(-Leu-Phe)] in aqueous solvent. This is achieved through a combination of all-atom molecular dynamics (MD) simulations, and field emission scanning electron microscopy (FESEM) experiments. Our aim is to investigate the differences that the retro-sequence of amino acids and the geometry of the dipeptides induce in their self-assembly propensity in aqueous solutions. Quantitative predictions of the peptide conformational, structural and dynamical properties at the molecular level as well as information regarding the end structure at the macroscopic level are presented. The two approaches allow us to explore a wide range of concentrations from high, often observed in atomistic simulations of biomolecules in explicit solvents due to system-size limitations, to low, commonly found in experiments due to peptide solubility issues.

The rest of the paper is divided into the following sections: Section II comprises systems and methods for both simulations and experiments; sections IIIA and IIIB comprise the results and section IV follow with discussion and concluding remarks.

II. Systems and Methods

a. Simulation Details

The model systems presented in this work are shown in Table 1. Details concerning the number of dipeptides (N_p), number of solvent molecules (N_s) and the total number of atoms in the system (N), as well as the size of the simulation box (L) and the simulation time (t_{sim}) are included. The concentration (c) is 38 mg(dipeptide)/ml(solvent) for all systems and the temperature (T) is constant at 300K.

All atom molecular dynamics simulations were performed using the GROMACS software⁴³. Solvent was described explicitly through the explicit single point charge SPC/E water model⁴⁴. Inter- and intramolecular interactions between atoms were described using the GROMOS54a7 force field⁴⁵⁻⁴⁷. The non-bonded interactions were parameterized through spherically truncated 6-12 Lennard-Jones potential and standard Lorentz-Berthelot mixing rules were used.

Table 1. Setup Details for the Simulated Systems

System	N_p	N_s	N	L (nm ³)	t_{sim} (ns)
Leu-Phe in H ₂ O	80	32011	98353	10x10x10	200
Phe-Leu in H ₂ O	80	32627	100201	10x10x10	250
Cyclo(-Leu-Phe) in H ₂ O	80	30060	92420	9.8x9.8x9.8	250

Simulations were performed in the isothermal–isobaric (NPT) statistical ensemble where the pressure was kept constant at $P=1$ atm using the Berendsen barostat⁴⁸, while the stochastic velocity rescaling thermostat⁴⁹ was used to maintain ambient temperature at $T=300$ K. The particle-mesh Ewald (PME) summation was used for the evaluation of long-range electrostatic interactions. The integration time step was 1.0 fs, and cutoff for non-bonded interactions was set at 10 Å. After creating randomly, the dipeptide configurations and adding the water molecules energy minimization was performed, followed by equilibration runs of ~ 50 ns. Then, production runs of about 0.25 μ s were executed. A model representation of the three dipeptides is shown in **Figure 1**.

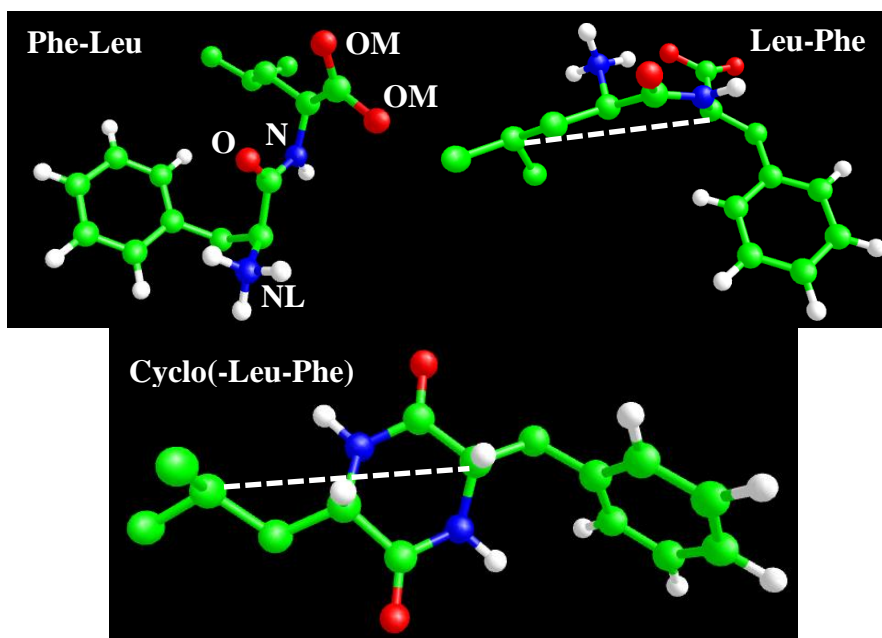


Figure 1: Model representation of dipeptide molecules. Characteristics vectors used for the orientational analysis are depicted with dotted lines.

Computation of PMF:

In general, the effective interactions between the dipeptides in water can be quantified by the (many-body) potential of mean force (PMF) which is given by the following equation:

$$U(Q) = -k_B T \log \int_{\Omega(Q)} e^{-U(q)/k_B T} dq, \text{ where } q=(q_1, q_2 \dots q_N) \text{ describe the positions of all atoms}$$

(N) of the system, and $Q=(Q_1, Q_2 \dots Q_N)$ are the coordinates of the center of mass (cm) of molecules. The integral is over all atomistic configurations that correspond to a given Q whereas V, T denote the volume of the system and the temperature accordingly. A common approximation of this demanding calculation is to estimate the potential of mean force through

$$\text{the calculation of the force: } F_i(Q) = -\frac{\partial U(Q)}{\partial Q_i} \quad i = 1, \dots, M ; \text{ acting on each molecule } I \text{ through}$$

the interactions with all other molecules (M) of the system. The many-body PMF is usually approximated by a two-body, pair, potential and a widely used procedure for its calculation is to perform constraint simulations of only two molecules in a solvent. In such simulations, the

distance between the centers of mass (cm) of the two molecules is kept constant throughout the entire simulation and the PMF ($U(r)$) is computed by integrating the mean force, $F(r)$, required to keep the two molecules at distance r , as follows: $U(r) = \int_{r_{\max}}^r F(r)dr - 2k_B T \ln r$; r_{\max} is the distance between the two molecules beyond which $U(r)$ equals to zero. The last term in the PMF formula is an entropic one, which corrects for the constraint of the cm–cm distance (i.e., it is required due to the rotation of the cms).

b. Experimental Details

All peptides were obtained from Bachem, Switzerland in the form of lyophilized powder and had a purity greater than 95%. Methanol solvent when required, was provided by Sigma-Aldrich and the water solvent used was nanopure purified, filtered and sterilized. Peptide solutions were prepared by dissolving at room temperature, the peptide powder into water, and methanol/water (3:7) at concentrations of $c=1$ mg/ml.

In the case of Cyclo(-Leu-Phe) dilution in pure water proved impossible and the two-solvent methanol/water (3:7) approach was used. Following methanol addition, the mixture was vortexed and placed in a water bath thermostat with a temperature of $T=50$ °C. Sonication was performed for 10 seconds with 20 seconds intervals for 15 minutes until complete dissolution was achieved, after which water addition took place to induce self-assembly.

For the Leu-Phe and Phe-Leu dipeptides water was added followed by vortex and brief 10-seconds sonication at 50-55 °C with 20 seconds intervals for two minutes. Dissolution was also possible without the use of temperature. A similar approach was also used in the case of the two-solvent methanol/water (3:7) systems. Post dilution, all peptide solutions were kept at ambient temperature for 24 h while a 10 μ l sample was collected immediately after dilution for FESEM visualization.

For FESEM observations, sample solutions of 10 μ L were collected at different time intervals of 0 min, 1 h, 2 h, 3 h, and 24 h after dilution with the moment of complete peptide dissolution counting as time 0. Samples (10 μ L) were then deposited on glass slides followed by 24h evaporation at room temperature. Prior to characterization, sputtering was performed for 64 seconds at 40 mA with (Au) layers at a thickness of 15 nm. The FESEM experiments

took place at the Biology Department of the University of Crete using a field-emission scanning electron microscope JEOL 7000, operating at 15 kV.

III. Results and Discussion

III.A Simulation Results

III.A.1 Effective Interactions

We start the analysis of the model dipeptides by investigating their tendency towards self-assembly in water, which is quantified through the calculation of the potential of mean force (PMF).

The pair PMF has been calculated for all three systems of dipeptides in water and results are presented in Figure 2. Attraction is apparent only in Leu-Phe and Cyclo(-Leu-Phe) systems, represented by the attractive well in the potential curves, while for Phe-Leu a fully repulsive potential is found. However differences are still observed between Cyclo(-Leu-Phe) and Leu-Phe, i.e. a deeper attractive well is found in Cyclo(-Leu-Phe), of the order of $\sim 3k_B T$, ranging between 0.5nm and 1nm, whereas in Leu-Phe the depth of the well is of the order of $\sim k_B T$ (i.e. comparable to thermal fluctuations), located at a similar r -range. As expected, for distances shorter than 0.5nm the repulsive interactions dominate, while beyond 1nm all effective interactions approach the zero value.

Moreover, based on the PMF data shown in Figure 2 it is clear that the attraction is the strongest in Cyclo(-Leu-Phe), indicating strong tendency for self-assembly among these molecules, Leu-Phe follows with a less strong self-assembly propensity, whereas no attraction is indicated among Phe-Leu dipeptides. PMF provides a first sign for the attraction between molecules in water. However, self-assembly is a collective phenomenon that requires further investigation which is presented below.

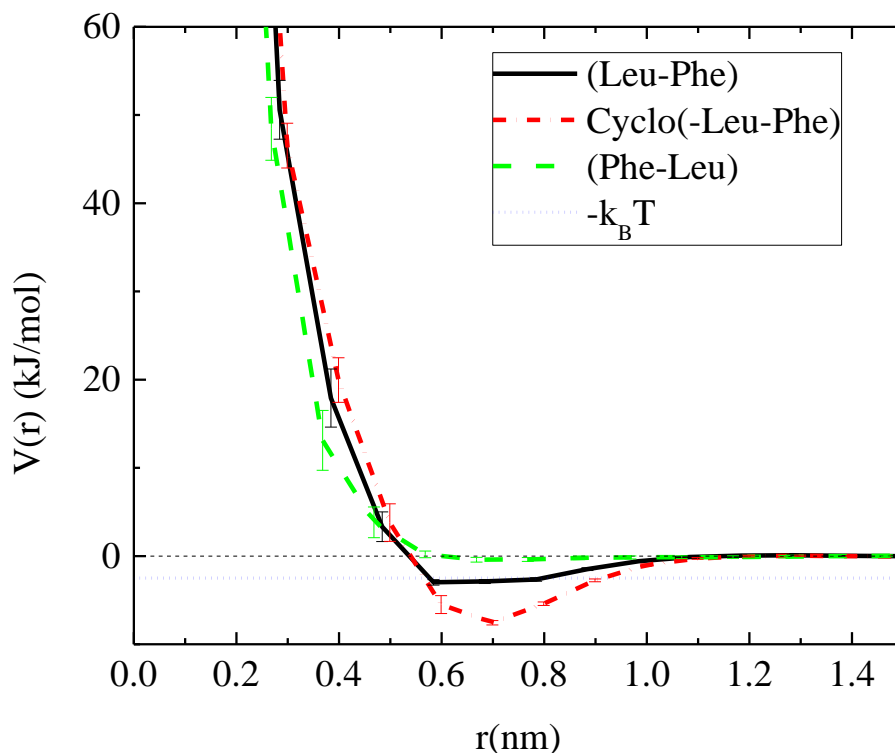


Figure 2: The potential of mean force (PMF) between Phe-Leu, Leu-Phe, and Cyclo(-Leu-Phe) dipeptides at 300K. Solid horizontal line corresponds to $k_B T$, thermal energy.

III.A.2 Structural and Conformational features

Next, we analyze the conformational and structural features of the dipeptides in aqueous solutions. A more detailed insight into the conformations of dipeptides, in the formed structures, can be provided by probing their preferred orientation relative to each other. To achieve this analysis on a pair of dipeptides for a series of constant cm-cm distances has been performed, based on the trajectories of the corresponding PMF runs. The preferable orientation is quantified by the dot product of two vectors defined along the backbone of each molecule, as presented schematically in Figure 1. The probability distribution of θ -value, $P(\theta)$, at different distances between the cms for all three dipeptides, is presented in **Figure 3a**, **3b** and **3c** for Leu-Phe, Phe-Leu and Cyclo(-Leu-Phe) respectively.

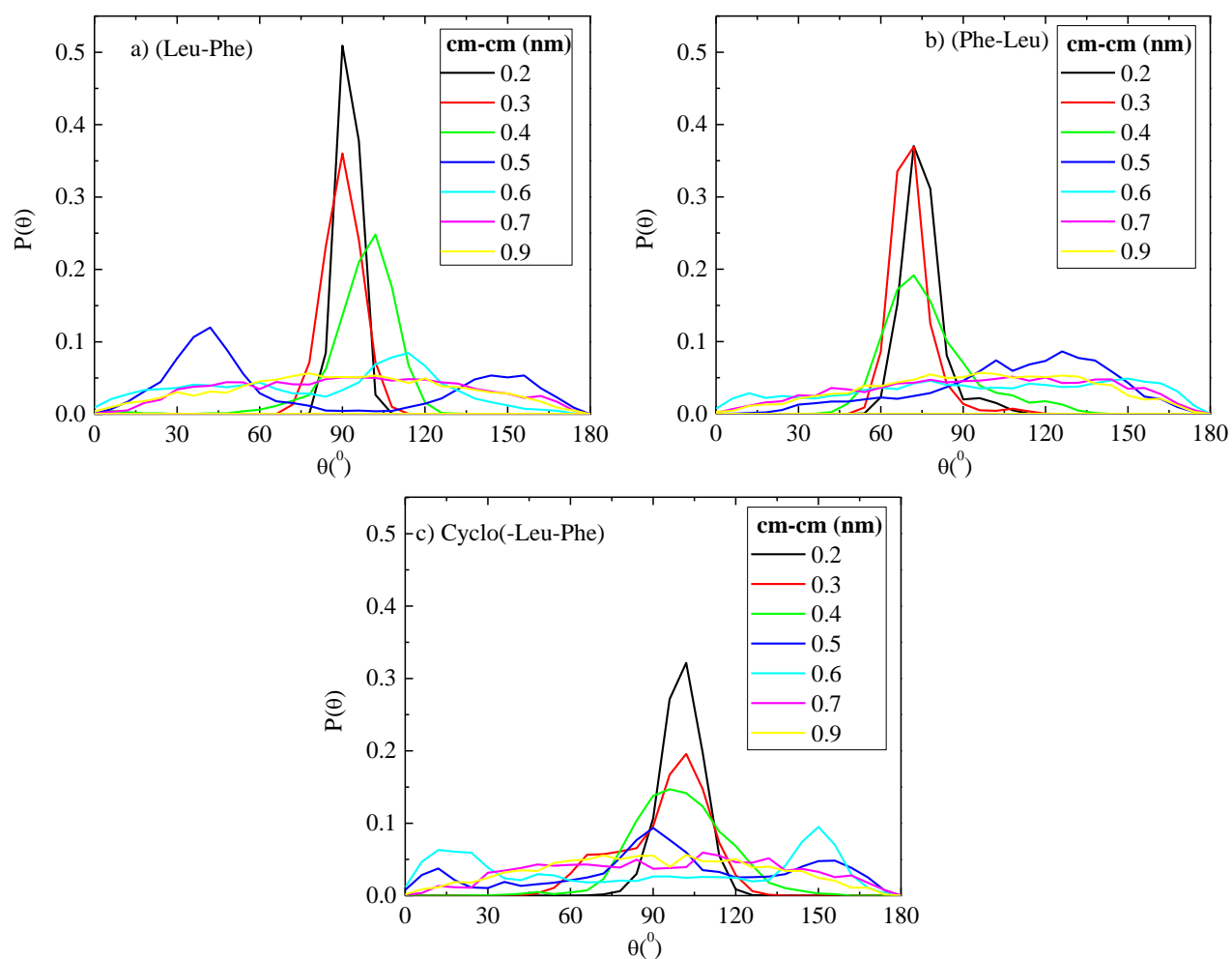


Figure 3: Probable orientations between a pair of Leu-Phe dipeptides in terms of angles between their backbone vectors (a) Leu-Phe; (b) Phe-Leu; (c) Cyclo(-Leu-Phe).

Starting from the retro-sequenced dipeptides (Figure 3a, 3b) a first difference in their orientation is observed at distances up to 0.4 nm. An almost normal orientation of the two molecules is observed for Leu-Phe, while their relative angle decreases in Phe-Leu to $\sim 70^\circ$. At these short distances the effort to reduce strong electrostatic repulsions determines the arrangement of the molecules, and this observation is an initial indication of different electrostatic interactions between the two dipeptides, as will be discussed in more detail below. Beyond 0.4 nm, broad θ -distributions indicate random orientation. Similar to Leu-Phe, for Cyclo(-Leu-Phe) dipeptides normal orientation is detected at very short cm-cm distances

~(0.2– 0.4)nm. As the distance between the centers of mass of the two dipeptides increases, molecules are inclined and their orientation is randomized. In contrast to diphenylalanine peptides where an antiparallel orientation of molecules is evident up to $\sim 0.6\text{nm}^4$ in the current aromatic-aliphatic dipeptides not any strong orientation preference is detected.

In the following all the results concerning static/structural properties, originate from data coming from simulations of aqueous solutions of dipeptides at $c = 38$ mg(dipeptide)/ml(solvent) (Table 1) and the analysis is based on the part of the trajectory in which the systems have reached a steady conformational state.

A typical measure which characterizes the local structure at the molecular level is the pair radial distribution function (rdf), $g(r)$, which is calculated in a solution of many molecules; however, it is a pair property closely related to the “conditional probability” to find two dipeptides one close to another. The rdfs between the center-of-mass of various dipeptides and between dipeptide and water molecules have been calculated for all systems and results are presented in Figure 4. The highest peak of rdf which corresponds to Cyclo(-Leu-Phe), followed by Leu-Phe and finally by Phe-Leu curve (Figure 4a) are in good agreement with the results from PMFs (Figure 2), assigning the strongest tendency for self-assembly to Cyclo(-Leu-Phe). Differences among the three dipeptides become more pronounced through this measure, i.e. rdf curve for Cyclo(-Leu-Phe) is not only much higher than the one which corresponds to Leu-Phe but wider as well, providing a rough estimation for the size of the formed aggregates in each system. The wider the curve the bigger the aggregate, which is the case of Cyclo(-Leu-Phe). Moreover, the tail of the curve, which tends to zero for large distances in Cyclo(-Leu-Phe), indicates assembly into a single aggregate of all dipeptides that exclude water molecules from their vicinity. On the contrary, for Leu-Phe rdf has a tail which tends to one for long distances indicating the existence of individual molecules or smaller aggregates of Leu-Phe distributed in the aqueous solution. In addition, the comparison of Leu-Phe with Phe-Leu system reveals a huge difference in the value of the first peak which is considerably shorter for the latter where tail values tend also to one.

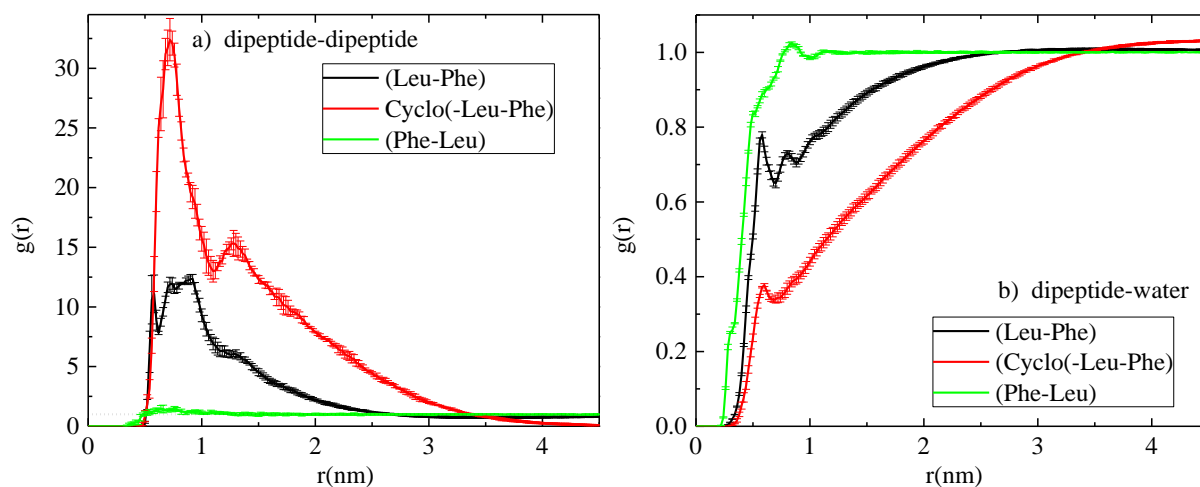


Figure 4: The pair radial distribution function (rdf) calculated for the cm of molecules in the aqueous solution at $T=300\text{K}$ (a) dipeptide - dipeptide and (b) dipeptide – water.

The above features signify a very weak propensity for self-assembly in Phe-Leu, in agreement with the corresponding PMF prediction. In Figure 4b the rdfs between dipeptide and water molecules show complementary to Figure 4a characteristics. The exclusion of water atoms from the vicinity of dipeptide is evident in Cyclo(-Leu-Phe) (i.e., very low values of the rdf at short distances). In Leu-Phe system a similar behavior is observed but less pronounced, while in Phe-Leu system an almost uniform distribution of water molecules is indicated from the corresponding rdf curve.

The aforementioned behavior supports a strong self-assembly propensity of Cyclo(-Leu-Phe) in water, milder in the case of Leu-Phe and almost none for the Phe-Leu dipeptides. In Figure 5 representative snapshots of the three systems verify the above discussion. The presented configurations correspond to typical molecular configurations in the steady state (time independent) region.

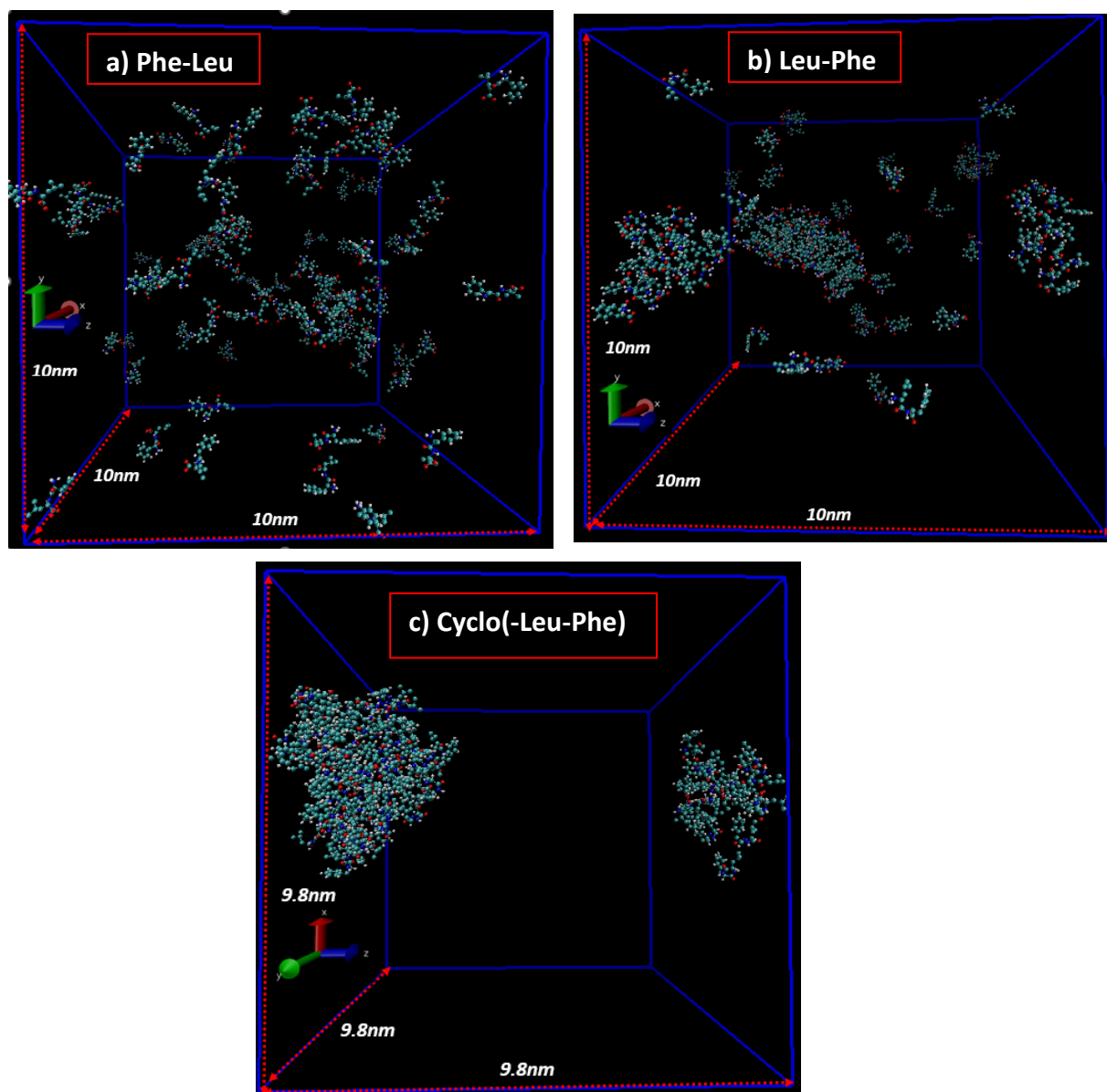


Figure 5: Characteristic snapshots from MD simulations of a) Phe-Leu; b) Leu-Phe and c) Cyclo(-Leu-Phe) dipeptides in aqueous solution. Water molecules are depicted as ghost molecules.

An almost spherical aggregate of Cyclo(-Leu-Phe) in water, consisting of all dipeptide molecules is found; moreover, smaller aggregates, formed by groups of Leu-Phe dipeptides, distributed in aqueous solution are observed. On the contrary, Phe-Leu dipeptides are rather

well dispersed throughout the solution, in agreement to the very weak attraction observed in the pair PMF data (see Figure 2). In all systems water molecules are omitted for clarity.

Conformational differences of individual dipeptides in the solution can be seen as a potential cause of the different behavior of the two retro dipeptides. The distributions of the dihedral angle along the peptide bond on the backbone of dipeptides can provide a measure for their conformational preferences. A corresponding Figure SI-1 for Leu-Phe and Phe-Leu is presented in the Supporting Information, where a clear difference is observed, with the angle for Phe-Leu dipeptide to attain a broader distribution compared to the one of Leu-Phe, indicating a larger variety of conformations. Representative snapshots of individual dipeptides, chosen randomly from the solution, are presented in Figure SI-2, which highlight these differences.

Furthermore, the size of individual dipeptides can be quantified by their mean radius of gyration: $\langle R_g \rangle = \sqrt{\left\langle \frac{\sum_i m_i (r_i - R_{cm})^2}{\sum_i m_i} \right\rangle}$, where r_i represents the coordinates of each atom i with mass m_i and R_{cm} is the center of mass of the molecule. Values for $\langle R_g \rangle$ are presented in Table 2 as an average over the equilibrated part of the trajectory. Phe-Leu and Leu-Phe are of quite similar size in vacuum (i.e., individual molecules) although a smaller size of Leu-Phe is observed in solution, which can be attributed to the self-assembly process that takes place in Leu-Phe. Moreover, the cyclic architecture results also in a small reduction of size in Cyclo(-Leu-Phe) compared to the two other dipeptides.

Table 2: The mean radius of gyration of all three dipeptides in aqueous solution:

System	$\langle R_g \rangle$ (nm)
Phe-Leu	0.362±0.002
Leu-Phe	0.320±0.001
Cyclo(-Leu-Phe)	0.304±0.002

Since aggregates are structures that are created and destroyed during the simulation due to energy fluctuations and their size, as well as their number vary, we examine the aggregation procedure by defining an “effective radius of gyration”, R_{geff} , based on the above formula of the radius of gyration, using the center of mass of all dipeptides in the system, taking into

account system's periodicity (i.e., minimum image convention) of a single molecule. We compute the average of R_{geff} over all molecules in the system, even if no aggregates exist. Consequently, in a uniformly distributed system R_{geff} will be equal to the half of the side of the cubic simulation box. Therefore, the smaller the value of R_{geff} , the more dipeptides form aggregates. R_{geff} values as a function of time for the three systems are presented in **Figure 6**. All curves start from a value almost equal to the half of the simulation box (see **Table 1**). For Cyclo(-Leu-Phe) (**Figure 6c**) R_{geff} is clearly a decreasing function of time, whereas beyond a specific time point, which also characterizes the time beyond which a steady conformational state is attained, it fluctuates around a constant value. A less pronounced decrease is observed in Leu-Phe curve (**Figure 6b**), where the attained constant value is much higher compared to Cyclo(-Leu-Phe). This is due to the formation of a single aggregate from all dipeptides in Cyclo(-Leu-Phe) in contrast to Leu-Phe where self-assembly propensity is weaker and more, smaller aggregates are formed. However, obviously self-assembly is not the case for Phe-Leu (**Figure 6a**), where R_{geff} fluctuates around a constant value throughout the simulation.

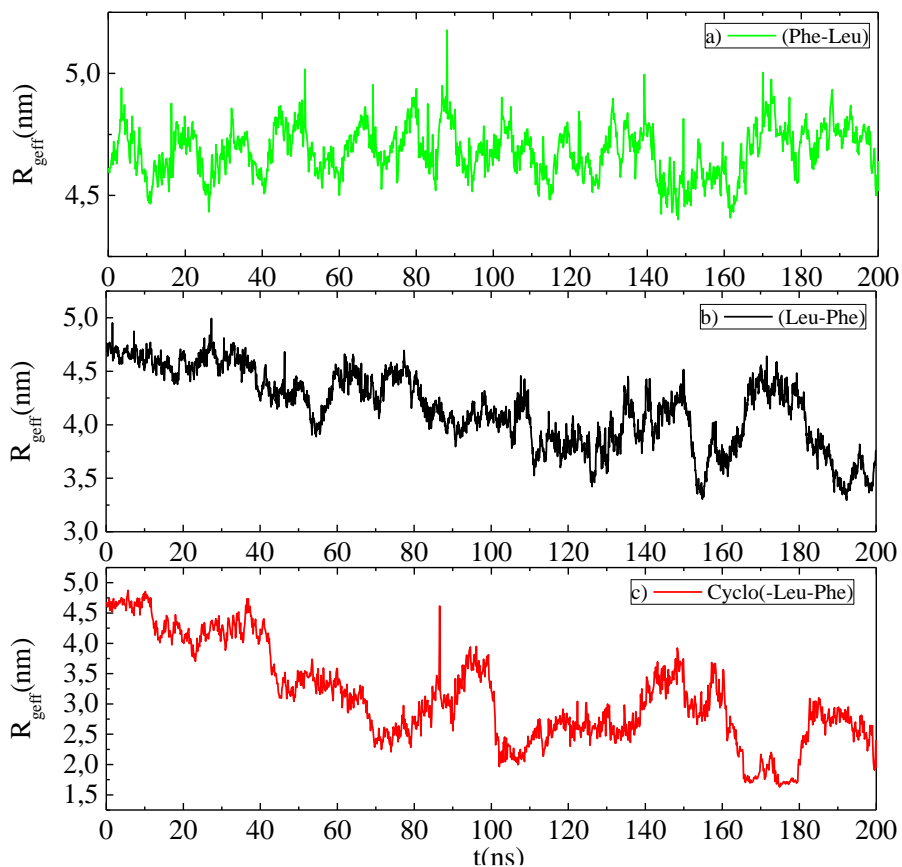


Figure 6: The effective radius of gyration as a function of time for the three systems. Note the different y-axis scaling which highlights the difference among curves.

Having reported the differences in the conformational properties among the three dipeptides the understanding of their origin is of particular interest. The proximity of the molecules in the assembled structures is determined by various factors. The molecule architecture and the compactness of the aggregate are two of them. In order to address this issue, two distinct comparisons are attempted; the first is between the cyclic dipeptide and its linear analogue and the second is between the dipeptide and its retro counterpart.

Conformational freedom is reduced in the cyclic architecture, which imposes bigger distances between atoms. This is expected to affect the mass distribution within the formed assemblies. Therefore, we monitor the assembly propensity of dipeptides and record the formed aggregates. Clusters of dipeptides of various sizes are detected. The compactness of these aggregates is quantified through the calculation of the average atom density measured as a function of the distance from the center of mass of the clusters. Results for atom density of Leu-Phe and Cyclo(-Leu-Phe) are presented in Figure 7. Comparison between the two curves reveals a density peak at shorter distances for the former dipeptide, indicating the concentration of atoms at closer distances and consequently more compact structures. This highlights the differences of the cyclic geometry as it is juxtaposed to its linear analogue whereas, at the same time, predisposes for different energetic interactions, as it will be discussed in the following.

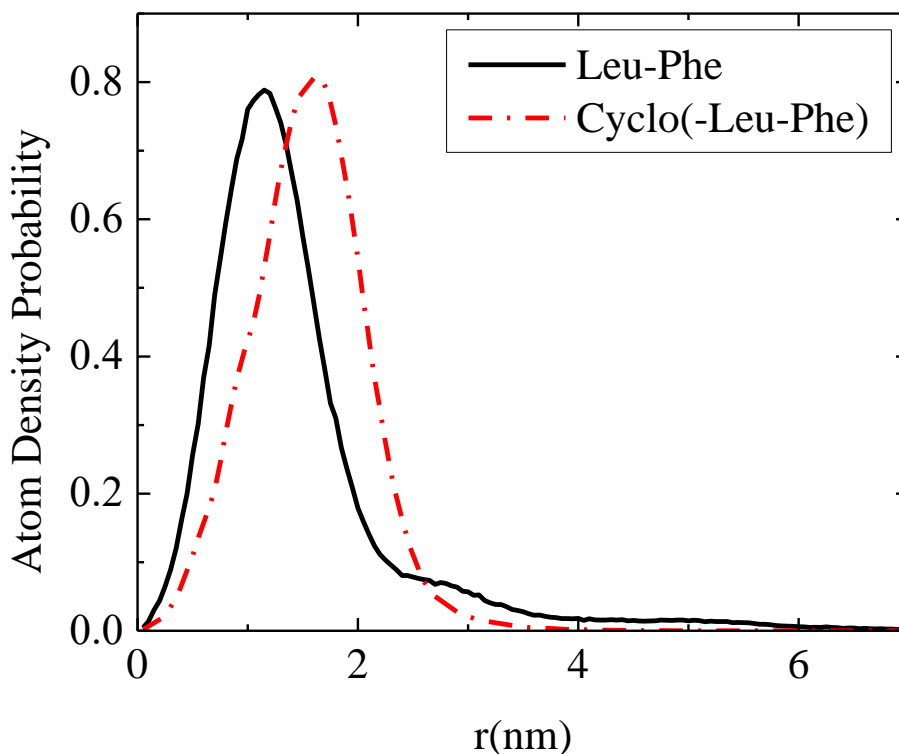


Figure 7: Average atom density probability of clusters as a function of the distance from their center of mass for Leu-Phe and Cyclo(-Leu-Phe).

Since the self-assembly tendency of Phe-Leu is very weak, the comparison of the dipeptides with reverse sequences will be based on energetic measures and is listed in the next subsection.

III.A.3 Self-Assembly Driving Forces

Hydrogen Bonds

In conjunction with hydrophobicity, a crucial interaction, which also drives the self-assembly propensity of dipeptides, is the hydrogen bonding. Hydrogen bonds are formed between all molecule types exist in the aqueous solution (i.e., dipeptide-dipeptide (P-P); dipeptide-water (P-W); water-water (W-W)). We have monitored hydrogen bonding for all systems and average values over the part of the trajectory in which the systems have reached a steady conformational state are listed in **Table 2**. The detection of hydrogen bonds is based on geometric criteria, namely the maximum distance between the hydrogen donor and the

acceptor to be 0.35nm and the angle formed by the Hydrogen-Donor-Acceptor triplet to be lower than 30° ⁵⁰. According to values presented in Table 2, hydrogen bonds between dipeptides per dipeptide in Cyclo(-Leu-Phe) system are double compared its linear analogue Leu-Phe. The positioning of atoms due to the cyclic geometry and the arrangement of molecules in the formed aggregates enhances the potential hydrogen bonding. Secondly, hydrogen bonds in Leu-Phe are significantly greater than in its reverse sequence dipeptide Phe-Leu. These results are in accordance to the degree of the self-assembly propensity as it has been observed through the various measures above.

A further analysis of hydrogen bonding is used in order to understand the origin of the differences observed between the two dipeptides of reverse sequence (i.e., Leu-Phe and Phe-Leu). We explore the propensity of head to tail interactions between the termini of two interacting dipeptides by measuring the corresponding hydrogen bonds which are presented in Table 3. Head to tail hydrogen bonding constitutes a percentage of ~28% of the total hydrogen bonds between dipeptides in Phe-Leu while, this percentage is only ~12% in Leu-Phe. This enhanced preference, percentage-wise, for head to tail arrangement of Phe-Leu explains the conformational differences between the assemblies formed by the two reverse dipeptides and is reflected also in the electrostatic interactions, presented below. Additionally, the pairs of hydrogen-bonding atoms are identified according to their code names which are presented in Figure 1. A comparison between the two dipeptides of reverse sequence is provided in order to discern which part of the molecule stops contributing to this process and as a result does not promote self-assembly. The average number of all hydrogen bonds of each corresponding pair is shown in Table 4. The differences are large for all pairs, but obviously, the reduction is huge for hydrogen bonds formed from the backbone atoms.

Table 3: Hydrogen bonds among all components in the aqueous solutions, number of water molecules in the vicinity of dipeptides and the percentage of the disturbance of hydrogen bond network of water for all systems:

System	HB (P-P)/P	HB (P-P)/P Head to Tail	HB (P-W)/P	HB (W-W) _{shell} /W _{shell}	N_{Water}	D(%)
Phe-Leu	0.06±0.03	0.017±0.03	9.78±0.20	1.36	8567.1	61.8
Leu-Phe	0.52±0.08	0.06±0.08	8.84±0.19	1.37	4756.8	61.3

Cyclo(- Leu-Phe)	1.11±0.07	-	1.92±0.10	1.43	1523.9	59.8
---------------------	-----------	---	-----------	------	--------	------

Table 4: Average number of hydrogen bonds among the potential pairs of hydrogen-bonding atoms for the two dipeptides of reverse sequence.

Atom Pairs	Leu-Phe	Phe-Leu
NL-OM	12.83	2.56
NL-O	3.08	0.84
N-OM	9.39	1.13
N-O	14.77	0.44

The hydrogen bonds between dipeptides and water molecules, which are shown in the third column of Table 3, have an opposite order compared to the number of hydrogen bonds between dipeptides. This value is highest for Phe-Leu, Leu-Phe follows closely, while in Cyclo(-Leu-Phe) a large decrease is observed consistent with the higher hydrophobicity of this dipeptide which leads to compact assembled structures.

In conjunction with the decrease of contacts with water for the dipeptides with the stronger self-assembly propensity, destruction in the hydrogen bond network of water molecules (N_{Water}) in the vicinity of dipeptides is observed. In order to quantify this destruction we define a spherical shell with radius equal to $1nm$ around each dipeptide and count the total number of hydrogen bonds around one dipeptide, which is equal to $HB = N_{Water} \times HB_{(W-W)shell/Wshell} + HB_{(P-w)/Wshell}$. The comparison with the number of hydrogen bonds between N_{Water} molecules in the bulk phase ($HB_{bulk} = N_{Water} \times \langle W-W \rangle / W$) reveals a percentage of the disturbance:

$\%D = \frac{|HB - HB_{bulk}|}{HB_{bulk}}$. Hydrogen bonds of pure water in bulk ($\langle W-W \rangle$) is equal to 3.56, in very

good agreement to the 3.6 value reported in the literature⁵¹. Results of the aforementioned calculations are presented in Table 3. The number of water molecules in a shell of $1nm$ radius is almost half in Leu-Phe compared to Phe-Leu, whereas in Cyclo(-Leu-Phe) is the one third compared to Leu-Phe. These values illustrate the degree of hydrophobicity of the respective dipeptides and thus the strength of their tendency for self-assembly. Noticeably, the resulting percentage of disturbance of hydrogen bonds network of water is comparable for all three systems at ~62% for Phe-Leu and Leu-Phe and slightly lower for Cyclo(-Leu-Phe) at ~60%.

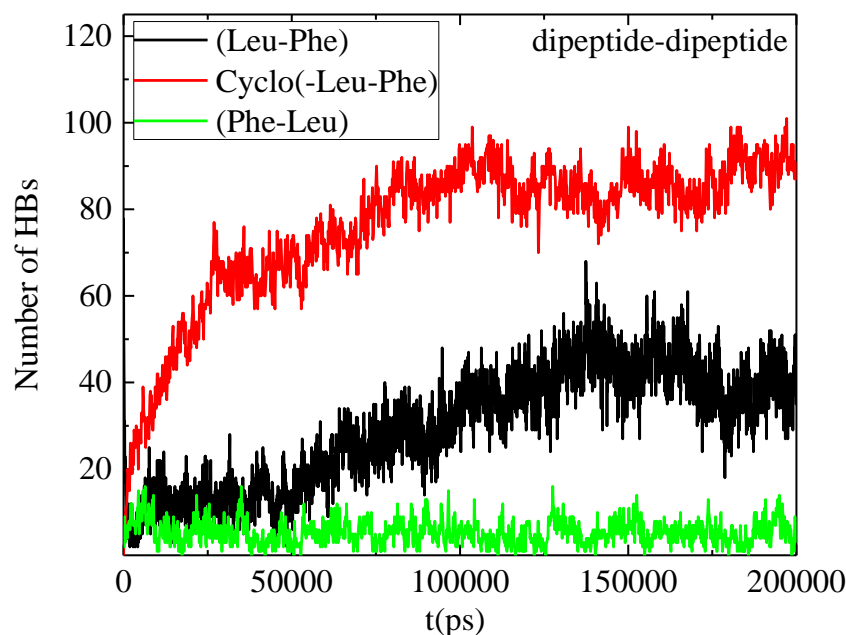


Figure 8: Hydrogen bonds between dipeptides as a function of time for the three systems.

The evolution of hydrogen bonding in time is presented in **Figure 8** providing an estimation for the kinetics of self-assembly procedure. The tendency for self-assembly leads to an increase of hydrogen bonds between dipeptides, starting from very small values, due to the uniformly distributed initial configurations. A relatively faster self-assembly kinetics is observed for the Cyclo(-Leu-Phe) (i.e., ~90ns) than the Leu-Phe ones, which is ~130ns. In Phe-Leu fluctuations around a small value are observed throughout the simulation. This behavior reflects a fast association process in Cyclo(-Leu-Phe) compared to the Leu-Phe, whereas no self-assembly is observed for the Phe-Leu, in agreement with their degree of hydrophobicity as discussed above (see also Figure 2).

The difference in the hydrophobicity between the two dipeptides of reverse sequence is further highlighted by the calculation of the pair radial distribution function between the phenyl rings for Leu-Phe and Phe-Leu, which is presented in Figure SI-3 in the Supporting Information. Differences between the two curves are similar with those of the total pair radial distribution functions (Figure 4) and indicate attenuated hydrophobicity in the case of Phe-Lue. Moreover, a histogram of the average distance between the side chains of Leu and Phe

respectively (hydrophobic groups), which includes both intra- and inter- molecular contributions, has been created and presented in Figure SI-4. This is in agreement with the overall self-assembly behavior showing a distribution centered at shorter distances in the case of Leu-Phe compared to Phe-Leu.

Electrostatic Interactions

In addition to hydrogen bonding, electrostatic interactions between dipeptides are often a critical driving force for the self-assembly propensity. We proceed to this calculation for all three systems in a part of their trajectory equal to 20ns, which corresponds to a steady conformational state. The short-range coulombic interaction among all atoms of dipeptides, according to their assigned charge is quantified, where greater attraction is expected when the molecules are a short distance apart. The considerable weaker self-assembly propensity excuses the big difference in the electrostatic energy for Phe-Leu compared to the other two systems. In addition, the more than twice the proportion of head-to-tail hydrogen bonding found in Phe-Leu, compared to its retro sequence (Leu-Phe), increases the spacing of atoms, resulting in lower electrostatic interactions. In the case of Cyclo(-Leu-Phe) compared to its linear analogue, although the PMF for the former has a deeper attractive well than the latter, electrostatic interactions are stronger for Leu-Phe. This can be attributed to the cyclic architecture which imposes bigger distances between atoms and as a consequence leads to looser aggregates (see Figure 7). Results for the coulombic interactions are presented in **Figure 9**. It is interesting to note that electrostatic attractions do not follow the strength of the for self-assembly propensity. This finding suggests the role of hydrogen bonding as prominent for the self-organization of the present systems.

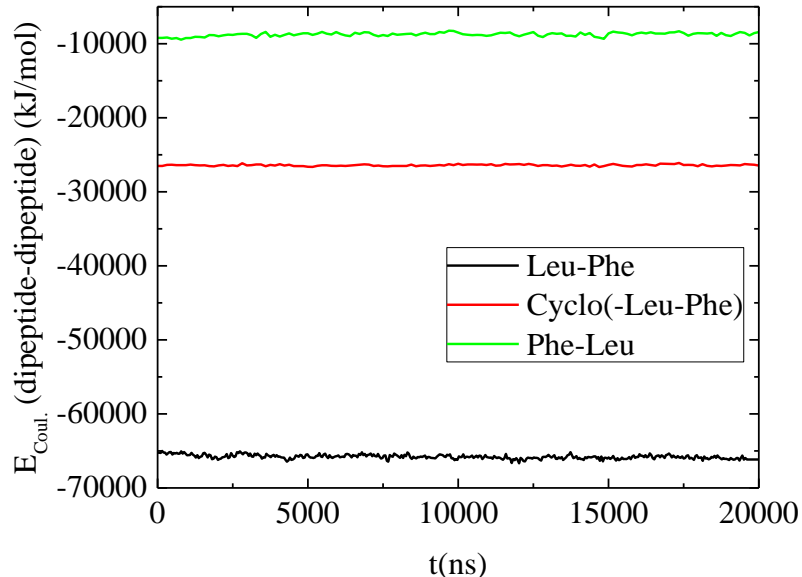


Figure 9: Coulombic interactions among dipeptides in aqueous solutions for all three systems.

III.B Experimental Results

Self-assembly of Leu-Phe, Phe-Leu:

We first examined the self-assembling tendency of Phe-Leu and Leu-Phe in pure water. Post-dissolution, no visible structures could be observed with the naked eye for neither peptide system, however upon solvent evaporation following deposition of 1 mg/ml peptide solution on glass slides, the Phe-Leu dipeptide would give rise to random irregular tube-like structures, of various sizes and formations with different openings symmetry-wise (**Figure 10a**). On the other hand well-formed fibrils could be observed in the case of Leu-Phe (**Figure 10b**) suggesting a more stable structure, probably as a result of stronger self-assembling tendency.

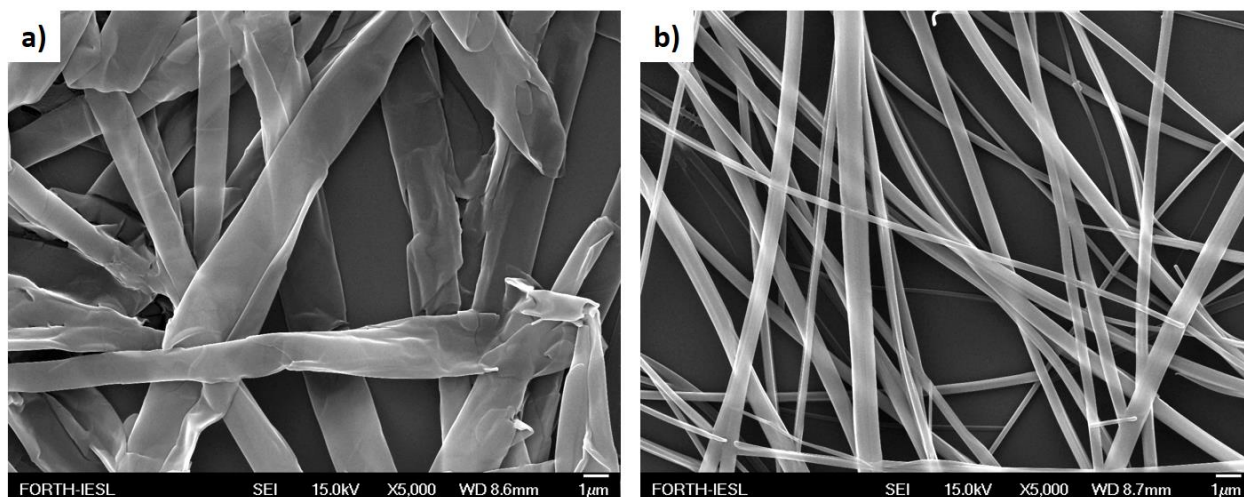


Figure 10: FESEM pictures of microstructures taken following H₂O evaporation after: 24h, at room temperature, at 1mg/ml for the following dipeptides: **a)** Phe-Leu, **b)** Leu-Phe.

Self-assembly of Cyclo(-Leu-Phe):

Due to its poor water solubility a methanol/water (3:7) system approach was used for Cyclo(-Leu-Phe). Visible formations could be detected right away inside the tubes which turned into hydrogels after 24h (**Supporting figure SI-5**). Post-solvent evaporation and deposition of 1 mg/ml Cyclo(-Leu-Phe) peptide solution on glass slides, various fibrillar networks with microscale diameter were observed (**Figure 11c**).

For the sake of comparison, the self-assembling tendency of Phe-Leu and Leu-Phe in the same solvent system was assessed. Phe-Leu would give rise to frayed ribbon/ tube-like structures (**Figure 11a**). Leu-Phe, following the exact same procedure of solvent evaporation on glass slide, would once more assemble into fibrils (**Figure 11b**). Pictures of these fibrillar structures taken at higher magnifications suggest a hollow, possibly microtubular nature (**Supporting figure SI-6**).

Since for both Leu-Phe and Cyclo(-Leu-Phe) cases the size distribution of the fibrillary formations varies, it is possible that while solvent evaporation might have an effect, self-assembly most probably is guided by small groups of molecule clusters acting as initiators while already formed fibrils and formations serve to increase the dimensional poly-dispersity of the fibrils. The observed Phe-Leu formations on the other hand, might be more affected by the solvent evaporation effect than their Leu-Phe and Cyclo(-Leu-Phe) counterparts due to their seemingly lower self-assembling tendency in solution as also observed computationally.

A comparative time course of all three peptides is presented in **Figure SI-7** indicating that the formations remain mostly the same, if only slightly more accentuated, over time.

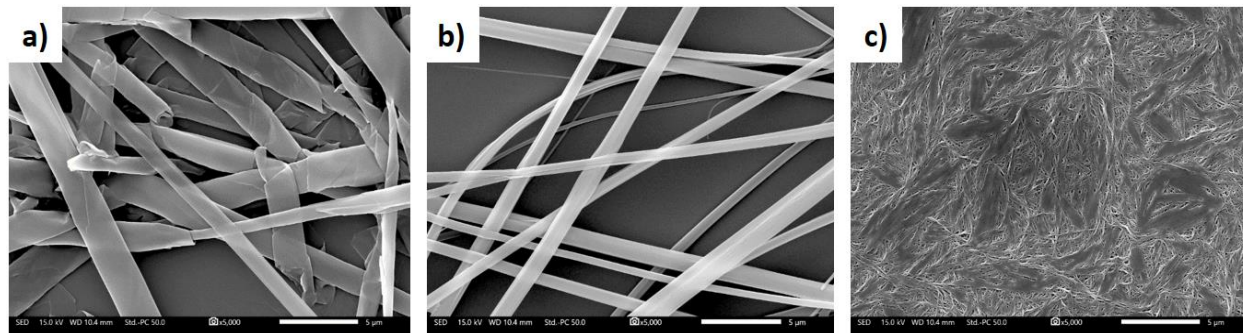


Figure 11: FESEM pictures of microstructures taken following MeOH/H₂O (3:7) evaporation after 24h, at room temperature, at 1mg/ml for the following dipeptides: a: Phe-Leu, b: Leu-Phe, c: Cyclo(-Leu-Phe). The Scale bar is 5 µm.

IV. Discussion and Conclusions

In this work, atomistic molecular dynamics simulations and FESEM experiments have been used in conjunction, in order to investigate the self-assembling tendencies of specific mixed aromatic-aliphatic dipeptides, i.e., Phe-Leu, Leu-Phe and Cyclo(-Leu-Phe) in aqueous solvent. These mixed aromatic/aliphatic dipeptides have not been widely investigated either theoretically or experimentally whereas, their distinct property is their frequent presence in neuropeptide sequences with Phe-Leu being the C-terminal motif in the enkephalin pentapeptide.

All-atom MD simulations were performed for the three systems at concentrations of 38mg/ml. In addition, end structures were observed using FESEM at concentrations of 1 mg/ml. While the explicit-solvent all-atom MD simulations provide quantitative predictions for conformational and dynamical self-assembling properties, through a detailed description of the atomic structure of the dipeptides, within the solvent, the field emission scanning electron microscopy experiments offer direct visualization of macroscopic structures and their morphology. Obviously, the differences in length and time scales between the computational and experimental approaches do not allow a one-to-one comparison of the respective findings.

The experimental structures are observed on the μm scale while the simulations cover a nm range. Therefore, the self-assembled aggregates observed in the model systems can be considered as precursors to the experimental structures in the limit of large numbers of dipeptides and possibly at much longer times. As such, despite the time-scale, size-scale and concentration differences between the two approaches, a qualitative comparison of their results showcases their complementarity.

Clear evidence of self-assembly was confirmed in the cases of Leu-Phe and Cyclo(-Leu-Phe) from both simulations and experiments, while the respective Phe-Leu dipeptide displayed a much lower self-organization propensity. We address the challenging task of unraveling the mechanisms governing self-assembly by analyzing how various factors affect the end morphologies. Furthermore, differences induced by the geometry of the molecules (i.e., linear vs cyclic), as well as by the reversing of their amino acid sequence are also highlighted.

The (pair) potential of mean force between dipeptide molecules constitutes the first evidence of self-assembly for Leu-Phe and Cyclo(-Leu-Phe), indicated by the presence of an attractive well in the potential curves, more pronounced for the later. On the contrary, the self-organization tendency of Phe-Leu seems negligible. The above is further supported by the high peaks of the pair-radial distribution functions observed between Leu-Phe and Cyclo(-Leu-Phe) peptides and the weak tendency of the Phe-Leu dipeptides to approach one-another, preferring to remain distributed inside the solution. In addition, hydrogen bonding suggests Cyclo(-Leu-Phe) as the dipeptide with the highest self-assembling propensity amongst all three dipeptides, while Phe-Leu displays the poorest. The significant role of hydrogen bonding in the self-assembly process is further highlighted by the calculation of the electrostatic interactions among dipeptide molecules. The strength of attraction follows the order Leu-Phe > Cyclo(-Leu-Phe) > Phe-Leu which is not the same with the strength of the self-assembly propensity. A high proportion of head-to-tail hydrogen bonds, with respect to the total number of hydrogen bonds, detected in Phe-Leu indicates conformations with more distant atoms compared to Leu-Phe. Moreover, hydrogen bonding between the backbone atoms is dramatically reduced in the former system. Additionally, the cyclic architecture of Cyclo(-Leu-Phe) imposes looser structures of aggregates than its linear counterpart (Leu-Phe). Both observations are consistent with the order of Coulomb interactions, while simultaneously highlighting important factors

affecting self-assembly. Moreover, the kinetics of the formation of hydrogen bonds is the fastest for Cyclo(-Leu-Phe), Leu-Phe follows whereas for Phe-Leu is the slowest.

Complementary information is provided by FESEM experiments which reveal large-scale assemblies and characterize the formed structures. In the case of Phe-Leu random and frayed ribbon/tube-like structures can be observed both in water and MeOH/water (3:7) systems, following solvent-evaporation. Given its apparently low self-assembling tendency in the solvent, our hypothesis is that the experimentally observed formations might be caused mainly by the dehydration and evaporation of the solvent from the glass slides with the glass surface also playing a role on the hierarchical organization of the formations³⁷.

On the other hand, Leu-Phe would always self-assemble into fibril-like formations of more consistent size and morphology in the solvents used, suggesting that they might be less affected by the evaporation effect in agreement with its higher self-organization propensity. Cyclo(-Leu-Phe) in accordance with its highest speculated self-assembling tendency, would give rise to hydrogel formations in MeOH/water (3:7) systems that consist of fibril-like networks, much like its behavior in certain other solvents as noted by S. Marchesan et al.^{31, 32} and others.^{29, 30}

The present study points to the differences in self-assembly propensity between linear, cyclic and retro-sequence peptides composed of the two same amino acids, Phenylalanine and Leucine as examined through a combination of simulations and experiments. The findings of the study can serve as stepping stone for applications that can be foreseen for the Phe-Leu based drugs. As mentioned above, Phe-Leu based dipeptide and tripeptide drugs act as proteasome inhibitors and are used for the treatment of multiple myeloma⁵². Despite the progress in the design and efficacy of proteasome inhibitors open issues remain, such as their formulation for controlled delivery, so the patients can avoid repeated injections. Hydrogel scaffolds such as the hydrogels formed by cyclo-Leu-Phe can serve as reservoirs for encapsulation and delivery of the aforementioned drugs. In that sense, the findings of the present study can pave the way for studying co-assembly of the carrier and the drug, both theoretically and experimentally and eventually, discover novel delivery routes.

This work showcases how simple alternations to the sequence's order or the peptide's own linear or cyclic nature, without the need for further modifications, can be an effective approach towards obtaining structurally and functionally different end-formations, facilitating the design

and increasing diversity of biocompatible materials, peptide therapeutics and their overall applications.

Supporting Information

Supplementary experimental data for the microstructure of dipeptides as well as the time evolution of their self-assembly are provided.

V. Acknowledgements

P.D. and A.M. research was co-financed by the European Union and Greek national funds through the Operational Program Competitiveness, Entrepreneurship, and Innovation, under the call RESEARCH – CREATE – INNOVATE (project Acronym : EPHESIAN, project code: T1EDK-01504).

MD simulations were performed on the Metropolis HPC facility of the Crete Center for Quantum Complexity and Nanotechnology.

We are grateful to Ms. Aleka Manousaki for assistance with FESEM experiments.

Notes

The authors declare no competing financial interest.

REFERENCES

- (1) Whitesides, G. M.; Grzybowski, B. Self-Assembly at All Scales. *Science* **2002**, *295* (5564), 2418-2421. DOI: 10.1126/science.1070821.
- (2) Reches, M.; Gazit, E. Casting metal nanowires within discrete self-assembled peptide nanotubes. *Science* **2003**, *300* (5619), 625-627, Article. DOI: 10.1126/science.1082387.
- (3) Adler-Abramovich, L.; Gazit, E. The physical properties of supramolecular peptide assemblies: from building block association to technological applications. *Chemical Society Reviews* **2014**, *43* (20), 6881-6893. DOI: 10.1039/C4CS00164H.

- (4) Rissanou, A. N.; Georgilis, E.; Kasotakis, E.; Mitraki, A.; Harmandaris, V. Effect of Solvent on the Self-Assembly of Dialanine and Diphenylalanine Peptides. *The Journal of Physical Chemistry B* **2013**, *117* (15), 3962-3975. DOI: 10.1021/jp311795b.
- (5) Yuan, C.; Li, S.; Zou, Q.; Ren, Y.; Yan, X. Multiscale simulations for understanding the evolution and mechanism of hierarchical peptide self-assembly. *Physical Chemistry Chemical Physics* **2017**, *19* (35), 23614-23631. DOI: 10.1039/C7CP01923H.
- (6) Gilead, S.; Gazit, E. Self-organization of Short Peptide Fragments: From Amyloid Fibrils to Nanoscale Supramolecular Assemblies. *Supramolecular Chemistry* **2005**, *17* (1-2), 87-92. DOI: 10.1080/10610270412331328943.
- (7) Rechtes, M.; Gazit, E. Designed aromatic homo-dipeptides: formation of ordered nanostructures and potential nanotechnological applications. *Physical biology* **2006**, *3* (1), S10-19. DOI: 10.1088/1478-3975/3/1/s02.
- (8) Gazit, E. A possible role for pi-stacking in the self-assembly of amyloid fibrils. *Faseb J* **2002**, *16* (1), 77-83. DOI: 10.1096/fj.01-0442hyp
- (9) Kokotidou, C.; Jonnalagadda, S. V. R.; Orr, A. A.; Seoane-Blanco, M.; Apostolidou, C. P.; van Raaij, M. J.; Kotzabasaki, M.; Chatzoudis, A.; Jakubowski, J. M.; Mossou, E.; et al. A novel amyloid designable scaffold and potential inhibitor inspired by GAIIG of amyloid beta and the HIV-1 V3 loop. *FEBS Letters* **2018**, *592* (11), 1777-1788. DOI: 10.1002/1873-3468.13096.
- (10) Hauser, C. A. E.; Deng, R.; Mishra, A.; Loo, Y.; Khoe, U.; Zhuang, F.; Cheong, D. W.; Accardo, A.; Sullivan, M. B.; Riekkel, C.; et al. Natural tri- to hexapeptides self-assemble in water to amyloid beta-type fiber aggregates by unexpected alpha-helical intermediate structures. *Proceedings of the National Academy of Sciences* **2011**, *108* (4), 1361-1366. DOI: 10.1073/pnas.1014796108.
- (11) Afonso, R.; Mendes, A.; Gales, L. Peptide-based solids: porosity and zeolitic behavior. *Journal of Materials Chemistry* **2012**, *22* (5), 1709-1723. DOI: 10.1039/C1JM13568F.
- (12) Comotti, A.; Fraccarollo, A.; Bracco, S.; Beretta, M.; Distefano, G.; Cossi, M.; Marchese, L.; Riccardi, C.; Sozzani, P. Porous dipeptide crystals as selective CO₂ adsorbents: experimental isotherms vs. grand canonical Monte Carlo simulations and MAS NMR spectroscopy. *CrystEngComm* **2013**, *15* (8), 1503-1507. DOI: 10.1039/C2CE26502H.

- (13) Moudrakovski, I.; Soldatov, D. V.; Ripmeester, J. A.; Sears, D. N.; Jameson, C. J. Xe NMR lineshapes in channels of peptide molecular crystals. *Proceedings of the National Academy of Sciences* **2004**, *101* (52), 17924-17929. DOI: 10.1073/pnas.0405348101.
- (14) Anedda, R.; Soldatov, D. V.; Moudrakovski, I. L.; Casu, M.; Ripmeester, J. A. A New Approach to Characterizing Sorption in Materials with Flexible Micropores. *Chemistry of Materials* **2008**, *20* (9), 2908-2920. DOI: 10.1021/cm8001805.
- (15) Soldatov, D. V.; Moudrakovski, I. L.; Ripmeester, J. A. Dipeptides as Microporous Materials. *Angewandte Chemie International Edition* **2004**, *43* (46), 6308-6311. DOI: 10.1002/anie.200460952.
- (16) Soldatov, D. V.; Moudrakovski, I. L.; Grachev, E. V.; Ripmeester, J. A. Micropores in Crystalline Dipeptides as Seen from the Crystal Structure, He Pycnometry, and ^{129}Xe NMR Spectroscopy. *Journal of the American Chemical Society* **2006**, *128* (20), 6737-6744. DOI: 10.1021/ja060474j.
- (17) Santos, S.; Torcato, I.; Castanho, M. A. R. B. Biomedical applications of dipeptides and tripeptides. *Peptide Science* **2012**, *98* (4), 288-293. DOI: 10.1002/bip.22067.
- (18) Fricker, L. D.; Margolis, E. B.; Gomes, I.; Devi, L. A. Five Decades of Research on Opioid Peptides: Current Knowledge and Unanswered Questions. *Mol. Pharmacol.* **2020**, *98* (2), 96-108, Review. DOI: 10.1124/mol.120.119388.
- (19) Mizushige, T.; Uchida, T.; Ohinata, K. Dipeptide tyrosyl-leucine exhibits antidepressant-like activity in mice. *Scientific Reports* **2020**, *10* (1), 2257. DOI: 10.1038/s41598-020-59039-7.
- (20) Mizushige, T.; Kanegawa, N.; Yamada, A.; Ota, A.; Kanamoto, R.; Ohinata, K. Aromatic amino acid-leucine dipeptides exhibit anxiolytic-like activity in young mice. *Neuroscience letters* **2013**, *543*, 126-129. DOI: 10.1016/j.neulet.2013.03.043.
- (21) Dill, K. A.; Ozkan, S. B.; Shell, M. S.; Weikl, T. R. The protein folding problem. *Annual review of biophysics* **2008**, *37*, 289-316. DOI: 10.1146/annurev.biophys.37.092707.153558
- (22) Tamamis, P.; Adler-Abramovich, L.; Reches, M.; Marshall, K.; Sikorski, P.; Serpell, L.; Gazit, E.; Archontis, G. Self-assembly of phenylalanine oligopeptides: insights from experiments and simulations. *Biophysical journal* **2009**, *96* (12), 5020-5029. DOI: 10.1016/j.bpj.2009.03.026.

- (23) Morrison, C. Constrained peptides' time to shine? *Nature Reviews Drug Discovery* **2018**, *17* (8), 531-533. DOI: 10.1038/nrd.2018.125.
- (24) Prasad, C. Bioactive cyclic dipeptides. *Peptides* **1995**, *16* (1), 151-164. DOI: 10.1016/0196-9781(94)00017-z.
- (25) Claro, B.; Bastos, M.; Garcia-Fandino, R. 4 - Design and applications of cyclic peptides. *Peptide Applications in Biomedicine, Biotechnology and Bioengineering*, Koutsopoulos, S. Ed.; Woodhead Publishing **2018**; pp 87-129. DOI:10.1016/B978-0-08-100736-5.00004-1
- (26) Arachchilage, A. P. W.; Wang, F.; Feyer, V.; Plekan, O.; Prince, K. C. Photoelectron spectra and structures of three cyclic dipeptides: PhePhe, TyrPro, and HisGly. *The Journal of chemical physics* **2012**, *136* (12), 124301. DOI:10.1016/B978-0-08-100736-5.00004-1
- (27) Colombo, G.; Curnis, F.; De Mori, G. M. S.; Gasparri, A.; Longoni, C.; Sacchi, A.; Longhi, R.; Corti, A. Structure-Activity Relationships of Linear and Cyclic Peptides Containing the NGR Tumor-homing Motif*. *Journal of Biological Chemistry* **2002**, *277* (49), 47891-47897. DOI: 10.1074/jbc.M207500200.
- (28) Li, L.; Xie, L.; Zheng, R.; Sun, R. Self-Assembly Dipeptide Hydrogel: The Structures and Properties. *Frontiers in Chemistry* **2021**, *9*, Review. DOI: 10.3389/fchem.2021.739791.
- (29) Hanabusa, K.; Matsumoto, Y.; Miki, T.; Koyama, T.; Shirai, H. Cyclo(dipeptide)s as low-molecular-mass gelling agents to harden organic fluids. *Journal of the Chemical Society, Chemical Communications* **1994**, (11), 1401-1402. DOI: 10.1039/C39940001401.
- (30) Hanabusa, K.; Matsumoto, M.; Kimura, M.; Kakehi, A.; Shirai, H. Low Molecular Weight Gelators for Organic Fluids: Gelation Using a Family of Cyclo(dipeptide)s. *Journal of Colloid and Interface Science* **2000**, *224* (2), 231-244. DOI: 10.1039/C39940001401.
- (31) Bellotto, O.; Kralj, S.; De Zorzi, R.; Geremia, S.; Marchesan, S. Supramolecular hydrogels from unprotected dipeptides: a comparative study on stereoisomers and structural isomers. *Soft Matter* **2020**, *16* (44), 10151-10157. DOI: 10.1039/D0SM01191F.
- (32) Scarel, M.; Marchesan, S. Diketopiperazine Gels: New Horizons from the Self-Assembly of Cyclic Dipeptides. *Molecules* **2021**, *26* (11), 3376. DOI: 10.3390/molecules26113376
- (33) Guo, Y.; Ying, J.; Sun, D.; Zhang, Y.; Zheng, M.; Ding, R.; Liu, Y.; Zhao, Y. Cyclic Dipeptides Formation From Linear Dipeptides Under Potentially Prebiotic Earth Conditions. *Frontiers in chemistry* **2021**, *9*, 675821. DOI: 10.3389/fchem.2021.675821.

- (34) Roxin, Á.; Zheng, G. Flexible or fixed: a comparative review of linear and cyclic cancer-targeting peptides. *Future Medicinal Chemistry* **2012**, *4* (12), 1601-1618. DOI: 10.4155/fmc.12.75.
- (35) Sugita, M.; Sugiyama, S.; Fujie, T.; Yoshikawa, Y.; Yanagisawa, K.; Ohue, M.; Akiyama, Y. Large-Scale Membrane Permeability Prediction of Cyclic Peptides Crossing a Lipid Bilayer Based on Enhanced Sampling Molecular Dynamics Simulations. *Journal of Chemical Information and Modeling* **2021**, *61* (7), 3681-3695. DOI: 10.1021/acs.jcim.1c00380.
- (36) Tao, K.; Chen, Y.; Orr, A. A.; Tian, Z.; Makam, P.; Gilead, S.; Si, M.; Rencus-Lazar, S.; Qu, S.; Zhang, M.; et al. Enhanced Fluorescence for Bioassembly by Environment-Switching Doping of Metal Ions. *Advanced Functional Materials* **2020**, *30* (10), 1909614. DOI: 10.1002/adfm.201909614.
- (37) Rissanou, A. N.; Simatos, G.; Siachouli, P.; Harmandaris, V.; Mitraki, A. Self-assembly of Alanine-Isoleucine and Isoleucine-Isoleucine Dipeptides through Atomistic Simulations and Experiments. *The Journal of Physical Chemistry B* **2020**, *124* (33), 7102-7114. DOI: 10.1021/acs.jpcc.0c03025.
- (38) Arnon, Z.; Vitalis, A.; Levin, A.; Michaels, T.; Caflisch, A.; Knowles, T.; Adler-Abramovich, L.; Gazit, E. Dynamic microfluidic control of supramolecular peptide self-assembly. *Nature Communications* **2016**, *7*. DOI: 10.1038/ncomms13190.
- (39) Jeon, J.; Shell, M. S. Self-Assembly of Cyclo-diphenylalanine Peptides in Vacuum. *The Journal of Physical Chemistry B* **2014**, *118* (24), 6644-6652. DOI: 10.1021/jp501503x.
- (40) Adler-Abramovich, L.; Aronov, D.; Beker, P.; Yevnin, M.; Stempler, S.; Buzhansky, L.; Rosenman, G.; Gazit, E. Self-assembled arrays of peptide nanotubes by vapour deposition. *Nature Nanotechnology* **2009**, *4* (12), 849-854. DOI: 10.1038/nnano.2009.298.
- (41) Li, N.; Qiu, S.; Fang, Y.; Wu, J.; Li, Q. Comparison of Linear vs. Cyclic RGD Pentapeptide Interactions with Integrin $\alpha\text{v}\beta\text{3}$ by Molecular Dynamics Simulations. *Biology* **2021**, *10* (7), 688. DOI: 10.3390/biology10070688
- (42) Wang, Y.; Kuczera, K. Molecular Dynamics Simulations of Cyclic and Linear DPDPE: Influence of the Disulfide Bond on Peptide Flexibility. *The Journal of Physical Chemistry* **1996**, *100* (7), 2555-2563. DOI: 10.1021/jp952669b.

- (43) Hess, B.; Kutzner, C.; van der Spoel, D.; Lindahl, E. GROMACS 4: Algorithms for Highly Efficient, Load-Balanced, and Scalable Molecular Simulation. *Journal of chemical theory and computation* **2008**, *4* (3), 435-447. DOI: 10.1021/ct700301q.
- (44) Chatterjee, S.; Debenedetti, P. G.; Stillinger, F. H.; Lynden-Bell, R. M. A computational investigation of thermodynamics, structure, dynamics and solvation behavior in modified water models. *The Journal of chemical physics* **2008**, *128* (12), 124511. DOI: 10.1063/1.2841127.
- (45) Berendsen, H. J. C.; Grigera, J. R.; Straatsma, T. P. The missing term in effective pair potentials. *The Journal of Physical Chemistry* **1987**, *91* (24), 6269-6271. DOI: 10.1021/j100308a038.
- (46) Oostenbrink, C.; Villa, A.; Mark, A. E.; van Gunsteren, W. F. A biomolecular force field based on the free enthalpy of hydration and solvation: the GROMOS force-field parameter sets 53A5 and 53A6. *Journal of computational chemistry* **2004**, *25* (13), 1656-1676. DOI: 10.1002/jcc.20090.
- (47) Schmid, N.; Eichenberger, A. P.; Choutko, A.; Riniker, S.; Winger, M.; Mark, A. E.; van Gunsteren, W. F. Definition and testing of the GROMOS force-field versions 54A7 and 54B7. *European Biophysics Journal* **2011**, *40* (7), 843-856. DOI: 10.1007/s00249-011-0700-9.
- (48) Berendsen, H. J. C.; Postma, J. P. M.; Gunsteren, W. F. v.; DiNola, A.; Haak, J. R. Molecular dynamics with coupling to an external bath. *The Journal of chemical physics* **1984**, *81* (8), 3684-3690. DOI: 10.1063/1.448118.
- (49) Bussi, G.; Donadio, D.; Parrinello, M. Canonical sampling through velocity rescaling. *The Journal of chemical physics* **2007**, *126* (1), 014101. DOI: 10.1063/1.2408420.
- (50) Luzar, A.; Chandler, D. Effect of environment on hydrogen bond dynamics in liquid water. *Physical review letters* **1996**, *76* (6), 928-931. DOI: 10.1103/PhysRevLett.76.928.
- (51) Kumar, R.; Schmidt, J. R.; Skinner, J. L. Hydrogen bonding definitions and dynamics in liquid water. *The Journal of chemical physics* **2007**, *126* (20), 204107. DOI: 10.1063/1.2742385.
- (52) Park, J. E.; Miller, Z.; Jun, Y.; Lee, W.; Kim, K. B. Next-generation proteasome inhibitors for cancer therapy. *Transl. Res.* **2018**, *198*, 1-16, Review. DOI: 10.1016/j.trsl.2018.03.002.

TOC graphic

